

Softness dependence of the Anomalies for the Continuous Shouldered Well potential

Pol Vilaseca and Giancarlo Franzese

Departament de Física Fonamental,

Facultat de Física, Universitat de Barcelona,

*Diagonal 647, 08028, Barcelona, Spain.**

(Dated: 30 March 2010)

arXiv:1004.3186v1 [cond-mat.soft] 19 Apr 2010

Abstract

By molecular dynamic simulations we study a system of particles interacting through a continuous isotropic pairwise core-softened potential consisting of a repulsive shoulder and an attractive well. The model displays a phase diagram with three fluid phases, a gas-liquid critical point, a liquid-liquid critical point, and anomalies in density, diffusion and structure. The hierarchy of the anomalies is the same as for water. Here we study in a systematic way the effect on the anomalies of varying the softness of the potential. We find that, making the soft-core steeper and more penetrable, the regions of density and diffusion anomalies contract in the $T - \rho$ plane, while the region of structural anomaly is weakly affected. Therefore, a liquid can have anomalous structural behavior without having density or diffusion anomalies. We show that, by considering as effective distances those corresponding to the maxima of the first two peaks of the radial distribution function $g(r)$ in the high-density liquid, we can generalize to continuous two-scales potentials a criterion for the occurrence of the anomalies of density and diffusion, originally proposed for discontinuous potentials. However, we observe that the knowledge of the structural behavior within the first two coordination shells of the liquid is not enough to establish, in general, the occurrence of the anomalies. By introducing the density derivative of the the cumulative order integral of the excess entropy, measuring shell by shell the amount of order in the liquid, we show that the anomalous behavior is regulated by the structural order at distances as large as the fourth coordination shell. By comparing the results for different softness of the potential, we conclude that the disappearing of the density and diffusion anomalies for the steeper potentials is due to a more structured short-range order. All these results increase our understanding on how, knowing the interaction potential, we can evaluate the possible presence of anomalies for a liquid.

PACS numbers: 64.70.Ja, 82.70.Dd, 61.20.Ja, 64.70.qj, 65.20.De

I. INTRODUCTION

Several liquids exhibit anomalous behaviours, i.e. behaviours that differ from what is expected for normal liquids such as argon. Water is the most common example of such systems. For example, while normal liquids contract when they are cooled, water expands under $T = 4^\circ C$ at ambient pressure¹.

However, water is not unique in this respect. The anomalous behavior in density, in fact, has been observed also in experiments for Bi^2 , Ga^2 , Te^3 , $S^{4,5}$, $Ge_{15}Te_{85}$ ⁶ and simulations for silica⁷⁻¹⁰, silicon¹¹ and BeF_2 ⁷. All these systems, including water, present a temperature of maximum density (TMD) below which density decreases when temperature is lowered at constant pressure.

Nevertheless, liquid water is anomalous also in other properties; for example, in its dynamics and its structure. While the diffusion coefficient D of a normal liquid decreases as density or pressure are increased, water is characterized by a region of the phase diagram where D increases when the pressure is increased. Experiments show that the normal behaviour is restored at pressures higher than $P \approx 1.1$ kbar at $283K$ ¹.

Regarding the structure, normal liquids tend to become more structured when compressed. This can be quantified by two order parameters: a translational order parameter t , quantifying the tendency of pairs of molecules to adopt preferential separations, and an orientational order parameter Q_l that measures the tendency of a molecule and its nearest neighbours to assume a specific local arrangement, as considered by Steinhardt et al.¹². For a normal liquid t and Q_l increase with pressure. Water, instead, shows a region where the structural order parameters decrease for increasing pressure or density at constant T , i.e. the system becomes more disordered, as shown by Errington and Debenedetti with molecular dynamics simulations¹³. Also simulations for a model of silica display similar anomalies, as shown by Shell et al.⁹.

The sequence of the anomalies in water is well determined in experiments¹ and simulations¹³. For the $T - \rho$ phase diagram the water structural anomaly region is encompassing the diffusion anomaly region which includes the density anomaly region.

Despite the fact that these anomalies can be found also in other liquids the sequence of anomalies may be different or may be the same. It is different, for example, for silica where the anomalous diffusion region contains the structural anomaly regions that, in turn,

includes the density anomaly region⁹. The sequence of anomalies is, instead, the same for several isotropic models¹⁴.

Isotropic models are systems of identical particles interacting through a central potential. It has been shown that isotropic potentials with a repulsive soft-core, either a ramp or a shoulder, have anomalies that resemble those of water^{15–43}.

Here we consider one of these potentials showing anomalies: the Continuous Shouldered Well potential (CSW), introduced in⁴⁴ and studied in detail in¹⁴. This model can be considered as the continuous version of the Discontinuous Shouldered Well potential (DSW) studied in^{40–43}. The two potentials have been shown to share the same qualitative phase diagram, with a liquid-liquid critical point in the supercooled liquid phase. However, while the CSW has anomalies, the DSW has not. The aim of the present study is to understand the origin of this difference. In particular, we tune the CSW potential in such a way to approximate, at least around the repulsive shoulder, the DSW, changing in this way the softness of the potential. Our results show that the continuous tuning of the CSW induces a continuous change on the regions of density and diffusion anomaly, but not a relevant effect on the structural anomaly region. When the CSW approaches the limit of the DSW, the regions of density and diffusion anomaly shrink as they would disappear.

The paper is organized as follows. We present the model in Sec. 2 and give details about the simulations in Sec 3. In Sec 4 we present our results about the phase diagram, and in Sec 5 our results about the anomalies, first with a criteria based on the excess entropy and then with a direct calculation. In Sec 6 we discuss the results, we generalize some proposed criteria and we study the effect of the long-range order. In Sec 7 we give our conclusions.

II. THE MODEL

We study the CSW model⁴⁴ consisting of a set of identical particles interacting through the isotropic pairwise potential given by

$$U(r) = \frac{U_R}{1 + \exp(\Delta(r - R_R)/a)} - U_A \exp\left[-\frac{(r - R_A)^2}{2\delta_A^2}\right] + \left(\frac{a}{r}\right)^{24} \quad (1)$$

where a is the diameter of the particles, R_A and R_R are the distance of the attractive minimum and the repulsive radius, respectively, U_A and U_R are the energies of the attractive well and the repulsive shoulder, respectively, δ_A^2 is the variance of the Gaussian centered in

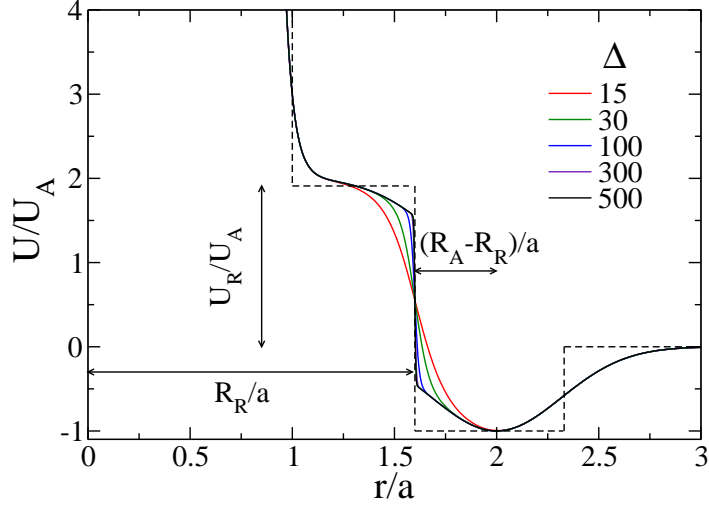


FIG. 1: Continuous lines represent the CSW potential for different values of the parameter Δ (slope at $r = R_R$). Dotted black line represents the discontinuous shouldered well potential (DSW)^{40–43}. By increasing the values of Δ the CSW potential tends to DSW around R_R .

R_A , and Δ is the parameter which controls the slope between the shoulder and the well at R_R (Fig. 1). Varying the parameters the potential can be tuned from a repulsive shoulder to a deep double well. In particular, by increasing Δ the soft-core repulsion becomes more penetrable near the minimum of the attractive well, and the softness of the potential increases for $r > R_R$ and decreases for $r < R_R$.

The set of values chosen for our analysis are as in^{14,44}, $U_R/U_A = 2$, $R_R/a = 1.6$, $R_A/a = 2$, $(\delta_A/a)^2 = 0.1$, while we tune Δ . In order to reduce the computational effort, we establish a cutoff for $U(r)$ at $r_c/a = 3$, because $U(r) \rightarrow 0$ for $r/a > 3$ for all the considered values of Δ . In particular, we consider the values $\Delta = 15, 30, 100, 300, 500$ (Fig. 1) going from the case $\Delta = 15$ studied in Ref.^{44,14} to slopes that approach the infinite value of DSW.

For $\Delta = 15$ this model is known to present anomalies in density, diffusion and structure^{14,44}. Its phase diagram displays a liquid-gas phase transition and a liquid-liquid phase transition, both ending in critical points^{14,44}.

III. MOLECULAR DYNAMICS

For every chosen value of Δ we simulate the behaviour of the system governed by the CSW potential using standard molecular dynamics techniques⁴⁵. We perform simulations in the NVT ensemble for $N = 1372$ particles interacting in a cubic box of volume V with periodic boundary conditions at temperature T . We use the Allen thermostat keeping T constant by rescaling the velocities of the particles at each time step by a factor $(T/\mathcal{T})^{\frac{1}{2}}$, where \mathcal{T} is the instantaneous kinetic temperature and T the fixed temperature of the thermal bath⁴⁶. We integrate the equations of motion using velocity Verlet integrator⁴⁶. By fixing ρ and T , we calculate the pressure in terms of the second virial coefficient⁴⁶. All calculations are presented in dimensionless reduced units in terms of the particle diameter and the depth of the attractive well: $P^* \equiv Pa^3/U_A$, $T^* \equiv k_B T/U_A$, $\rho^* \equiv \rho a^3$, and $D^* \equiv D(m/a^2 U_A)^{1/2}$, where D is the diffusion coefficient.

We use a simulation time step $\delta t^* = 3.2 \times 10^{-3}$ defined in units of $(a^2 m/U_A)^{1/2}$ (of the order of $\approx 1.7 \times 10^{-12} s$ for water-like molecules and $\approx 2.1 \times 10^{-12} s$ for argon-like atoms). Simulations are equilibrated after 10^4 time steps, followed by 10^6 time steps during which thermodynamic quantities are computed every 100 time steps. Positions and velocities are stored every 1000 time steps for the calculations of structure and dynamic quantities. For each value of ρ^* and T^* we average over two runs, starting from independent configurations.

Near the liquid-liquid critical point (described in the next section) we observe that the liquid phase is metastable with respect to the crystal phase. The nucleation of the crystal is marked by a subsequent drop in the potential energy⁴¹. The lifetime of the metastable phase is defined as the time between the end of the equilibration and the energy drop.

IV. THE PHASE DIAGRAM

First we verify that our simulations reproduce the known phase diagram for the model with $\Delta = 15^{14,44}$. Next, we calculate the phase diagram for the other considered values of Δ , finding always the same qualitative behaviour (Fig.2). In particular, we find two regions with coexisting fluid phases: (i) gas and liquid at low ρ^* , (ii) low density liquid (LDL) and high density liquid (HDL) at higher ρ^* . The two coexistence regions end in critical points: C_1 for gas-liquid coexistence, C_2 for LDL-HDL coexistence (Table I). For $\Delta < 100$ the HDL

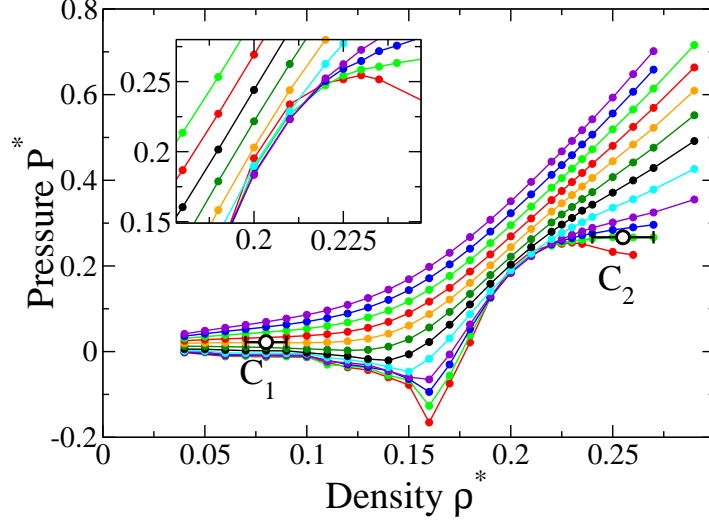


FIG. 2: Isotherms in the $P^* - \rho^*$ phase diagram from simulations for CSW potential with $\Delta = 30$ (from top to bottom, $T^* = 1.4, 1.3, 1.2, 1.1, 1.0, 0.9, 0.8, 0.7, 0.6, 0.55, 0.5$ and 0.45). At low T^* , isotherms have no monothonic behaviour and show two van der Waals loops, corresponding to a liquid-gas (low densities) and a liquid-liquid (higher densities) first order phase transitions both ending in critical points (C_1 and C_2 respectively). Inset: the crossing of the isotherms signals the presence of the density anomaly. In this and the following figures errors, where not shown, are smaller than symbol size.

phase is metastable with respect to the crystal, but with a lifetime long enough to allow us to equilibrate the liquid around C_2 . For $\Delta \geq 100$ the HDL lifetime is too short to equilibrate the liquid around C_2 and we extrapolate the location of C_2 from higher T^* isotherms.

As Δ is increased both C_1 and C_2 tend to the corresponding values for the DSW potential. This result is consistent with the idea that the DSW can be seen as a limiting case of the family of CSW potentials studied here. However, temperature and pressure of the LDL-HDL critical point for $\Delta = 500$ are still far from the values for the DSW potential.

V. HIERARCHY OF THE ANOMALIES FOR DIFFERENT Δ

Barros de Oliveira et al.¹⁴ show that the CSW potential has anomalies in density, diffusion and structure. Furthermore, they found a hierarchy of the anomalies as reported for other two-scale potentials and for the SPC/E water. Here we study in a systematic way how these

	$T_{C_1}^*$	$P_{C_1}^*$	$\rho_{C_1}^*$	$T_{C_2}^*$	$P_{C_2}^*$	$\rho_{C_2}^*$
$\Delta = 15$	0.95 ± 0.06	0.019 ± 0.008	0.08 ± 0.03	0.49 ± 0.01	0.285 ± 0.007	0.247 ± 0.008
$\Delta = 30$	1.01 ± 0.07	0.022 ± 0.008	0.08 ± 0.03	0.50 ± 0.01	0.267 ± 0.005	0.255 ± 0.009
$\Delta = 100$	1.06 ± 0.04	0.025 ± 0.005	0.08 ± 0.03	0.53 ± 0.02	0.243 ± 0.005	0.262 ± 0.008
$\Delta = 300$	1.06 ± 0.05	0.027 ± 0.009	0.09 ± 0.02	0.51 ± 0.01	0.231 ± 0.007	0.271 ± 0.008
$\Delta = 500$	1.08 ± 0.06	0.027 ± 0.008	0.09 ± 0.03	0.52 ± 0.01	0.204 ± 0.007	0.272 ± 0.008
DSW	1.24 ± 0.01	0.030 ± 0.001	0.09 ± 0.02	0.69 ± 0.02	0.110 ± 0.002	0.280 ± 0.020

TABLE I: Temperatures $T_{C_1}^*$ and $T_{C_2}^*$, pressures $P_{C_1}^*$ and $P_{C_2}^*$, densities $\rho_{C_1}^*$ and $\rho_{C_2}^*$ (in reduced units) corresponding to the gas-liquid critical points C_1 and the LDL-HDL critical point C_2 , respectively, for different values of Δ for the CSW potential. We estimate the critical parameters by using the condition $(\partial^2 P / \partial \rho^2)|_T = 0$ at C_1 and C_2 . We confirm the data for $\Delta = 15$ from Ref.^{14,44}. For sake of comparison, we indicate also the values for the DSW potential with parameters $U_R/U_A = 2$, $R_R/a = 1.6$, $R_A/a = 2$, and $(\delta_A/a)^2 = 0.1$ from Ref.^{40–43}

anomalies depend on the parameter Δ of the CSW potential. In Fig. 3 we summarize all our results. In the next subsections we discuss the details of Fig. 3.

A. Excess entropy

As a starting point for the exploration of the anomalous regions of the potential and in order to predict whether a given anomaly will appear, we perform an analysis of the excess entropy. The excess entropy s^{ex} is defined as the difference between the entropy s of a real fluid at a given T and ρ and the entropy of an ideal gas s^{ig} under the same conditions, $s^{\text{ex}} \equiv s - s^{\text{ig}}$, and quantifies the entropy lost due to interactions and correlations between the particles of the fluid. It has been shown that the excess entropy allows an approximate estimate of the regions where density, diffusion and structure are anomalous. In particular, Errington et al.⁴⁷ proposed that the condition under which the density anomaly appears is given by $\Sigma_{\text{ex}} > 1$, where by definition is $\Sigma_{\text{ex}} \equiv (\partial s^{\text{ex}} / \partial \ln \rho)_T$. The diffusion anomaly can also be predicted, following Rosenfeld’s empirical parametrization⁴⁸, by the condition $\Sigma_{\text{ex}} > 0.42$. Structural anomaly is determined by the criterion $\Sigma_{\text{ex}} > 0$, because for normal

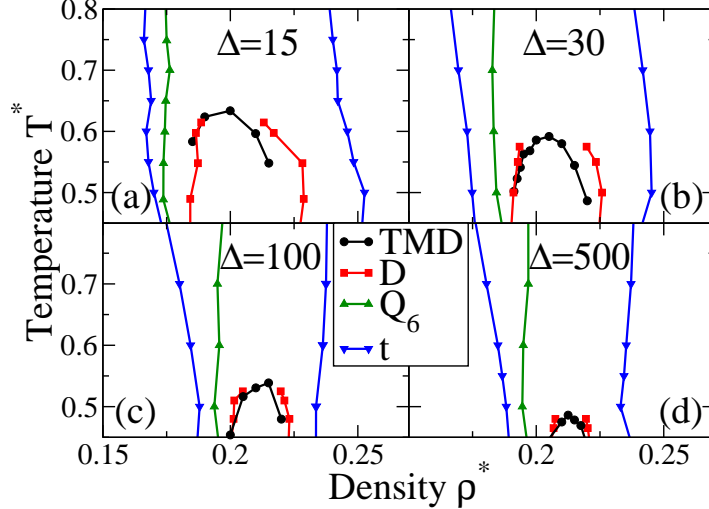


FIG. 3: Hierarchy of anomalies (as defined in Sec. V) in the $T^* - \rho^*$ plane, plotted for (a) $\Delta = 15$, (b) $\Delta = 30$, (c) $\Delta = 100$ and (d) $\Delta = 500$. As the value of Δ increases, both the regions of density anomaly (\bullet) and diffusion anomaly (\blacksquare) contract with the diffusion anomaly region always encompassing the TMD line. The region of structural anomaly (between \blacktriangle -symbols for Q_6 maxima and the high- ρ^* \blacktriangledown -symbols for t minima) is only weakly affected.

fluids the excess entropy is always decreasing when density increases isothermally⁴⁹.

The evaluation of the excess entropy might be computationally expensive. However, it can be approximated directly by the two-body contribution term

$$s_2 \equiv -2\pi\rho \int [g(r) \ln g(r) - g(r) + 1] r^2 dr \quad (2)$$

which depends only on the radial distribution function and represents the dominant contribution to the excess entropy⁴⁸⁻⁵¹ (between 85% and 95% of s^{ex} for a Lennard-Jones fluid^{51,52}). Since the integrand of Eq.(2) goes to zero for large r , i.e. where $g(r)$ goes to 1, we calculate s_2 up to a cutoff given by half the simulation-box size, distance at which we check that $g(r) \approx 1$ within the range of T and ρ considered in this work. From Eq.(2) we define and calculate $\Sigma_2 \equiv (\partial s_2 / \partial \ln \rho)_T$. We observe that the predicted regions of anomalies get narrow as the slope Δ increases (Fig. 4).

Since $s_2 < s^{\text{ex}}$, then it is always $\Sigma_{\text{ex}} < \Sigma_2$. Therefore, the criteria $\Sigma_2 > 1$, $\Sigma_2 > 0.42$ and $\Sigma_2 > 0$ overestimate the regions of density, diffusion and structural anomalies, respectively, with about 30% uncertainty, according to Rosenfeld⁴⁸. As we will discuss in Section VI, we observe that the anomalous regions predicted in Fig. 4 are indeed an overestimate of the one

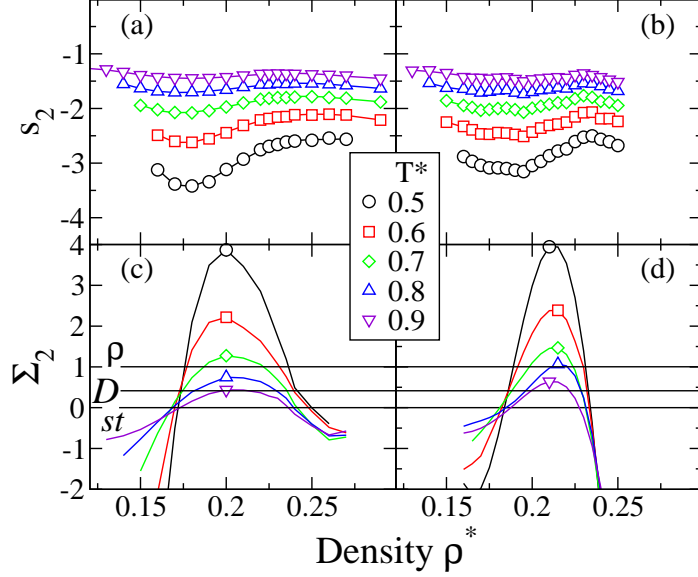


FIG. 4: Excess entropy s_2 (upper panels) and its derivative Σ_2 (lower panels) for the potentials corresponding to $\Delta = 30$ (left panels) and $\Delta = 500$ (right panels), for $T^* = 0.5$ (\circ), 0.6 (\square), 0.7 (\diamond), 0.8 (\triangle), 0.9 (∇). Horizontal solid lines in the bottom panels are the thresholds for Σ_2 for the anomalies (from top to bottom for density, diffusion and structural anomaly, respectively). As described in the text, these criteria overestimate the regions of anomalies.

we find as a result of the detailed analysis presented in the next sections. Nevertheless, the approximate criteria based on Σ_2 give a preliminary idea of where the anomaly occur.

B. The density anomaly

For all the considered values of Δ , we find a temperature of minimum pressure along the isochores near the LDL-HDL critical point C_2 (Fig. 5). These temperatures correspond to the TMD line at constant P . We find that the anomalous region where ρ decreases for decreasing T shrinks for increasing Δ and possibly tends to collapse onto one single point in the $P^* - T^*$ plane for $\Delta \rightarrow \infty$. This result would be consistent with the behaviour of the DSW potential, that does not show density anomaly^{40–43}.

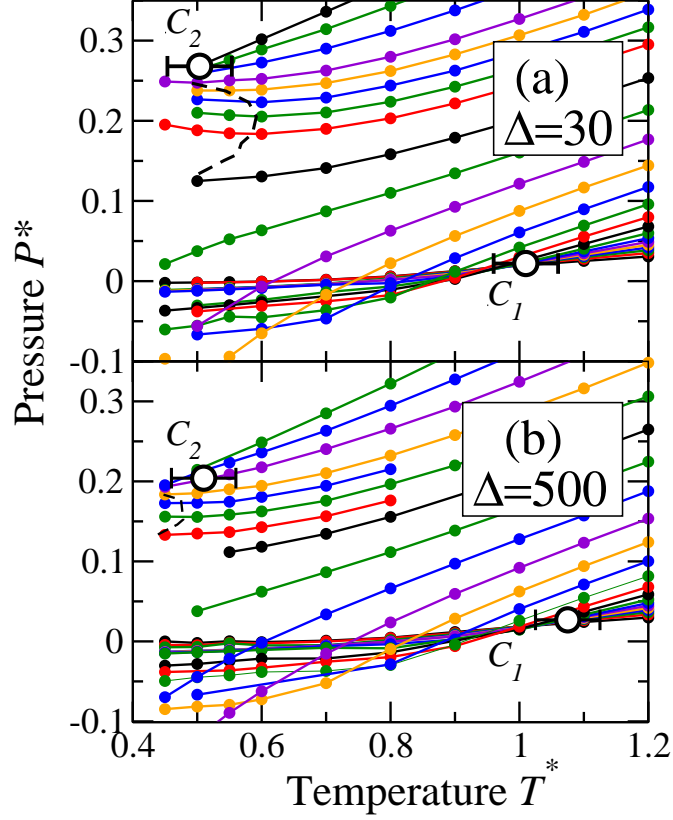


FIG. 5: The $P^* - T^*$ phase diagram for $\Delta = 30$ (a) and $\Delta = 500$ (b). In both panels, we show isochores (with constant density separation $\delta\rho^* = 0.01$) from $\rho^* = 0.04$ (at high T^* and low P^*) to 0.20, from 0.205 to 0.215 (with $\delta\rho^* = 0.005$), and (with $\delta\rho^* = 0.01$) from 0.22 to 0.25 (at low T^* and high P^*). The points where isochores cross correspond to the gas-liquid and LDL-HDL critical points (C_1 and C_2 , respectively). The black dashed line is a guide for the eye estimating the TMD line, corresponding to the line of minima along the isochores.

C. Diffusion anomaly

For the family of potentials given by Eq. (1) with the considered values of Δ we find an anomalous-diffusion region, i.e. a region ($\rho_{Dmin} < \rho < \rho_{Dmax}$) where D increases with increasing density at constant T (Fig. 6). The diffusion coefficient is calculated from the mean square displacement of a single particle

$$\langle \Delta r(t)^2 \rangle \equiv \langle [r(t_o + t) - r(t_o)]^2 \rangle, \quad (3)$$

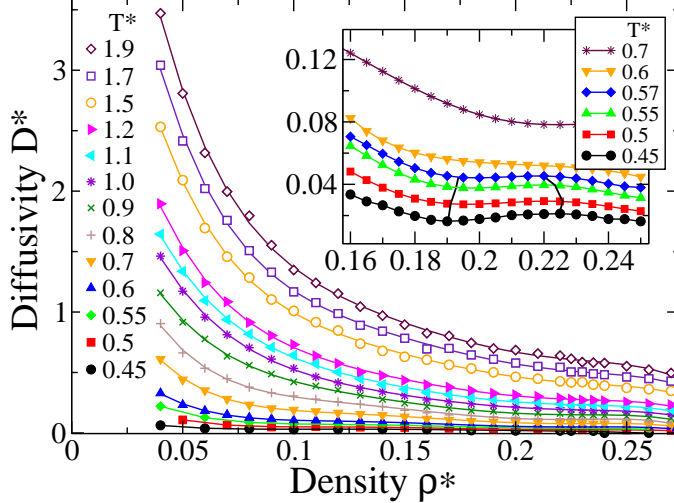


FIG. 6: Diffusion coefficient D^* as a function of density ρ^* for $\Delta = 30$ and isotherms from $T^* = 0.45$ (bottom) to $T^* = 1.9$ (top). Inset: Isotherms from $T^* = 0.45$ (bottom) to $T^* = 0.7$ (top) Black solid lines delimit the anomalous region where D^* grows from D_{\min} to D_{\max} for increasing density between $\rho_{D_{\min}}^* < \rho^* < \rho_{D_{\max}}^*$.

where t_o is any time at equilibrium and the average is over the initial t_o and over the particles in the system, taking the long-time limit

$$D = \lim_{t \rightarrow \infty} \frac{\langle \Delta r(t)^2 \rangle}{2dt} \quad (4)$$

where $d = 3$ is the dimension of the system. We find that as in the case of the density anomaly, the region of diffusion anomaly contracts as Δ increases. We find that the diffusion anomaly region always encompasses the TMD line between $\rho_{D_{\min}}$ and $\rho_{D_{\max}}$ (Fig. 3).

D. Structural anomaly

The structural behaviour of the system is studied by calculating the translational order parameter t and the orientational order parameter Q_6 defined in the following. The translational order parameter is defined as^{9,13,53}

$$t \equiv \int_0^\infty |g(\xi) - 1| d\xi \quad (5)$$

where $\xi \equiv r\rho^{1/3}$ is a reduced distance (in units of the mean interparticle separation $\rho^{-1/3}$) and $g(\xi)$ is the radial distribution function. Since in our simulations $g(\xi) \simeq 1$ for $\xi \geq \xi_c = 8$,

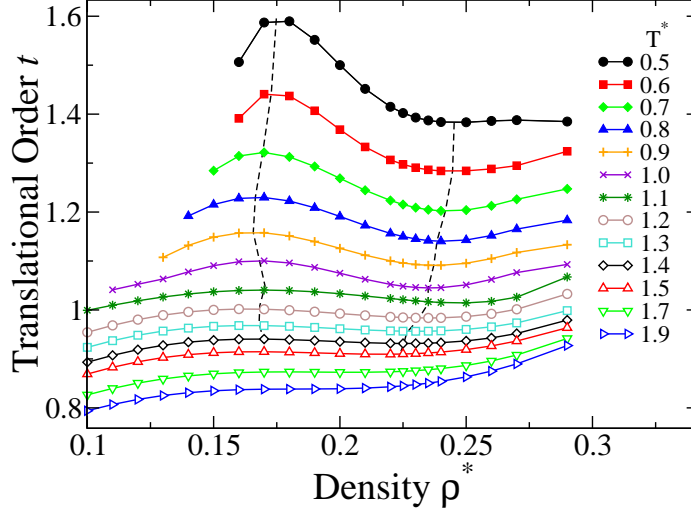


FIG. 7: Translational order parameter t as a function of density ρ^* for $\Delta = 30$ and isotherms from $T^* = 0.5$ (top) to $T^* = 1.9$ (bottom). Dotted lines joining the maxima and minima along the isotherms are a guide for the eye delimiting the region between $\rho_{t_{\max}}$ and $\rho_{t_{\min}}$, where t decreases for increasing ρ^* .

we integrate up to a cutoff distance ξ_c . As the parameter t depends only on the deviations of $g(\xi)$ from unity, its value is sensible to long range periodicities. For an ideal gas $g(\xi)$ is constant and equal to 1 and there is no translational order ($t = 0$). For a crystal phase $g(\xi) \neq 1$ for long distances and t becomes large. While normal fluids show a monotonic increase of t with increasing density, for the CSW potential t increases for $\rho < \rho_{t_{\max}}$, and reaches a maximum at $\rho_{t_{\max}}$. Above $\rho_{t_{\max}}$, for increasing ρ , t decreases until it reaches a minimum at $\rho_{t_{\min}}$. For $\rho > \rho_{t_{\min}}$, t recovers the normal behaviour (Fig. 7).

The local orientational order for a particle i and an index l is defined as¹²

$$Q_l^i \equiv \left[\frac{4\pi}{2l+1} \sum_{m=-l}^{m=l} |(\bar{Y}_{lm}^i)_k|^2 \right]^{1/2} \quad (6)$$

where k is a fixed number of nearest neighbour particles and $(\bar{Y}_{lm}^i)_k \equiv \frac{1}{k} \sum_{j=1}^k Y_{lm}(r_{ij})$ is the average of the spherical harmonics Y_{lm} with indices l and m , evaluated over the vectorial distance r_{ij} between particles i and j .

The calculations involved in the evaluation of Q_l^i can be computationally expensive. In order to reduce the computational effort, we express the spherical harmonics in terms of the

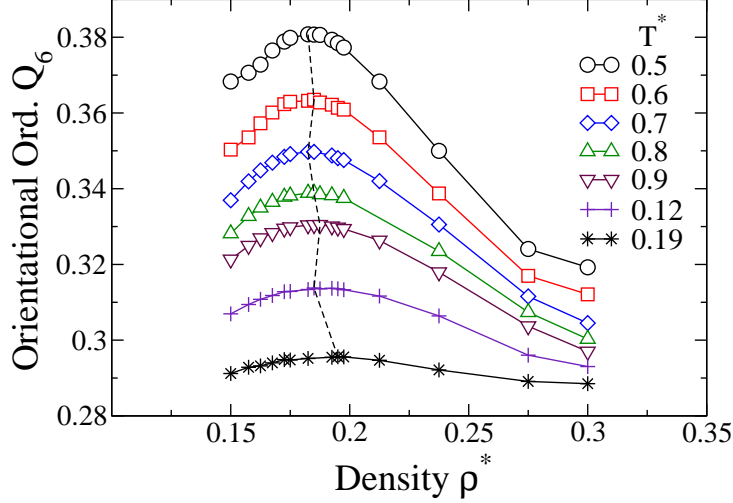


FIG. 8: Orientational order parameter Q_6 as a function of ρ^* for $\Delta = 30$, for isotherms going from $T^* = 0.5$ (top) to $T^* = 1.9$ (bottom). The dotted line is a guide for the eye joining the maxima along the isotherms.

Legendre Polynomials P_l obtaining

$$Q_l^i = \frac{1}{\sqrt{k}} \left[1 + \frac{2}{k} \sum_{j=1}^{k-1} \sum_{h=j+1}^k P_l(\cos \gamma_{jh}^i) \right]^{1/2}, \quad (7)$$

where γ_{jh}^i is the angle formed by the vectors \vec{r}_{ij} and \vec{r}_{ih} .

A global order parameter is obtained by averaging the local order Q_l^i over all particles

$$Q_l \equiv \frac{1}{N} \sum_{i=1}^N Q_l^i. \quad (8)$$

We study the case $l = 6$ and $k = 12$ as in Ref.⁵⁴. For $l = 6$ the sixth order Legendre Polynomial is given by $P_6(x) = \frac{1}{16} (231x^6 - 315x^4 + 105x^2 - 5)$. For an isotropic homogeneous system, Q_6 reaches its minimum value $Q_6^{\text{ih}} = 1/\sqrt{k} = 0.287$ ($k = 12$), while for a fully ordered f.c.c arrangement $Q_6^{\text{fcc}} = 0.574$.

The normal behaviour of Q_6 for a fluid without anomalies is to increase monotonically when ρ^* increases at constant T^* , or when T^* decreases at constant ρ^* . Q_6 decreases to the value Q_6^{ih} at high T^* . For the CSW potential, Q_6 has a non-monotonic behaviour along the isotherms with a maximum at $\rho_{Q_{\text{max}}}$ (Fig. 8).

The density $\rho_{Q_{\text{max}}}$ for each isotherm lies between $\rho_{t_{\text{max}}}$ and $\rho_{t_{\text{min}}}$. In the area between $\rho_{Q_{\text{max}}}$ and $\rho_{t_{\text{min}}}$ both order parameters decrease for increasing ρ , hence the liquid gets more

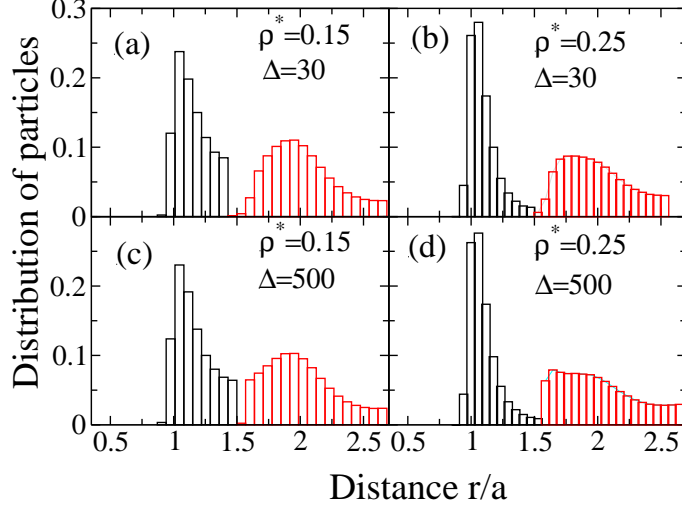


FIG. 9: Particle distribution for the first and second peaks of the $g(r)$, normalized by the area of each peak, at $T^* = 0.5$: for $\Delta = 30$ at (a) $\rho^* = 0.15$ and (b) $\rho^* = 0.25$, and for $\Delta = 500$ at (c) $\rho^* = 0.15$ and (d) $\rho^* = 0.25$. The distance between the maxima of the first and the second peak decreases for increasing ρ and for increasing Δ .

disordered with increasing density. This behaviour defines the structural anomaly region ($\rho_{Q_{\max}} \leq \rho \leq \rho_{t_{\min}}$).

By increasing the value of Δ we find that the region of structural anomaly does not contract, but tends asymptotically to a fixed region in the $T^* - \rho^*$ plane (Fig. 3). This weak dependence on Δ suggests that the occurrence of the structural anomaly does not disappear for very steep soft-core potentials. This prediction is consistent with the s_2 calculations that allow de Oliveira et al.¹⁴ to argue that the structural anomaly should be observable also for the DSW potential, here considered as the limit of the CSW for $\Delta \rightarrow \infty$.

VI. DISCUSSION

To get more insight into the origin of the anomalies, we study the relation between the changes of the coordination shells of the radial distribution function $g(r)$ and the appearance of the anomalies. First, we perform a systematic study of the first two peaks of $g(r)$. For example, for $\Delta = 30$ we find that at densities within the LDL phase (Fig. 9a) the distribution of particles of the first peak is maximum at $r_1/a \simeq 1.05$, next to the hard-core. For the second peak, the distribution is maximum at $r_2/a \simeq 1.95$, at about the minimum of the

attractive well. At densities within the HDL phase many particles overcome the shoulder approaching the hard-core. For $\rho^* = 0.25$ (Fig. 9b) the maximum of the first peak increases without changing its position, at $r_1/a \simeq 1.05$, while the distribution of the second peak is slightly flattened with a maximum around $r/a \simeq 1.75$. This change by increasing density shows that particles in the attractive well of the potential accumulate close to the soft-core distance, giving rise to an asymmetric distribution of particles around the minimum of the attractive well.

For the highest Δ considered here, $\Delta = 500$, we find a similar result at the LDL density (Fig. 9c), but at the density $\rho^* = 0.25$ (Fig. 9d), approaching the LDL-HDL critical point, the distribution of particles at the second peak⁵⁷ displays a flat region in the range $1.7 \leq r/a \leq 2.0$ and a maximum around the soft-core distance at $R_R/a = 1.6$. This is consistent with the fact that for $\Delta = 500$ the potential has a more penetrable soft-core for $r/a > 1.6$ with respect to the case $\Delta = 30$. As a consequence, the effective soft-core distance for the potential with $\Delta = 500$ is smaller than that for the potential with $\Delta = 30$.

This qualitative observation gives rise to a quantitative criterion for the prediction of the occurrence of the density and diffusion anomaly when we generalize what has been proposed by Yan et al. for potentials with a repulsive ramp⁵⁸. They observe that, if a and b are respectively the starting and ending distance of the repulsive ramp, the anomalies of density and diffusion occur only when $0.5 < a/b < 6/7 = 0.86$. This is consistent with the fact that for real water in standard conditions the ratio between the distances of the first two peaks of the oxygen-oxygen $g(r)$ is about 0.6, while in normal liquids it is about 0.5⁵⁸.

A straightforward application of the the Yan's criterion to our case is not obvious. One could assume that the relevant ratio in the CSW potential is $a/R_A = 0.5$, or as an alternative $R_R/R_A = 0.8$. With both choices one would conclude that Yan's criterion does not hold for the CSW potential because it would always predict the absence (with the first choice) or the occurrence (with the second choice) of the anomalies independently on Δ .

Hence, to generalize the Yan's criterion to cases in which the effective soft-core distance changes with density or Δ , as in the present case, we adopt as characteristic length-scales the maxima of the first two peaks of the $g(r)$ within the HDL phase and define the ratio $\lambda(\Delta) \equiv r_1(\rho)/r_2(\rho)|_{\rho_{\text{HDL}}}$ at a temperature below, or at about, the LDL-HDL critical point. The ratio λ is larger for more penetrable potentials, i. e. for larger Δ in the case of the CSW potential.

With this generalized definition, we conclude that the empirical criterion proposed by Yan et al.⁵⁸ is valid also for all the cases considered in our work. For the cases in Fig. 9 it is, for example, $\lambda(\Delta = 30) = 0.55 < \lambda(\Delta = 500) \simeq 0.66$, where the approximation symbol is used because for $\Delta = 500$ we can evaluate λ only at densities approaching $\rho_{\text{HDL}}(T)$.⁵⁷ We observe that by increasing λ the regions in the plane $(T - \rho)$ where the density and diffusion anomalies occur reduce in a sensible way, while the region of structural anomalies is almost unaffected by the change of λ (Fig. 3).

The considerations above are possibly consistent with the idea that the structure within the first two coordination shells is controlling the occurrence of the anomalies. In the following we will show that this concept is not leading to any general criterion for the occurrence of the anomalies and that the anomalies are, instead, regulated by the structure at a larger scale.

To this goal, we test an idea proposed in Ref.⁵⁹ suggesting that a necessary condition for the appearance of the anomalies is a transference of particles from the second shell of the fluid to the first shell under isothermal compression. According to this criterion all the anomalies appear for the range of ρ and T where

$$\Pi_{1,2} \equiv \left. \frac{\partial g(r)}{\partial \rho} \right|_{r_1} \times \left. \frac{\partial g(r)}{\partial \rho} \right|_{r_2} < 0, \quad (9)$$

i. e. Eq.(9) is a necessary condition. On the other hand, if $\Pi_{1,2} \geq 0$, no anomalies should be observed, i. e. the condition in Eq.(9) is also sufficient.⁵⁹

To study the implications of Eq. (9), we analyse the behaviour of the CSW $g(r)$ upon isothermal compression (Fig. 10 and Fig. 11). For all the considered values of Δ and ρ^* we find that it is always $\Pi_{1,2} < 0$, even for T and ρ outside the regions of the anomalies. Therefore, the condition in Eq. (9) could be necessary, but not sufficient, for the appearance of the anomalies. This observation is consistent with the result for the DSW potential, where Eq. (9) is satisfied (see Fig. 17 in Ref.⁴¹) but no density anomaly is observed⁴⁰⁻⁴³.

To understand better why Eq. (9) is not a sufficient condition for the anomalies, we study how $\Pi_{1,2}$ changes with ρ and T (Fig. 12). For each T , we find that $\Pi_{1,2}(\rho)$ is not monotonic, consistent with the fact that $\Pi_{1,2}(\rho)$ is expected to be negative around the anomaly regions and to be positive at smaller and larger ρ . We observe that $\Pi_{1,2}(\rho)$ reaches a lower minimum for lower T , i. e. $\Pi_{1,2}$ is more negative where the anomalies are stronger. However, away from its minimum $\Pi_{1,2}(T)$ is not a monotonic function of T at constant ρ . Moreover, we find

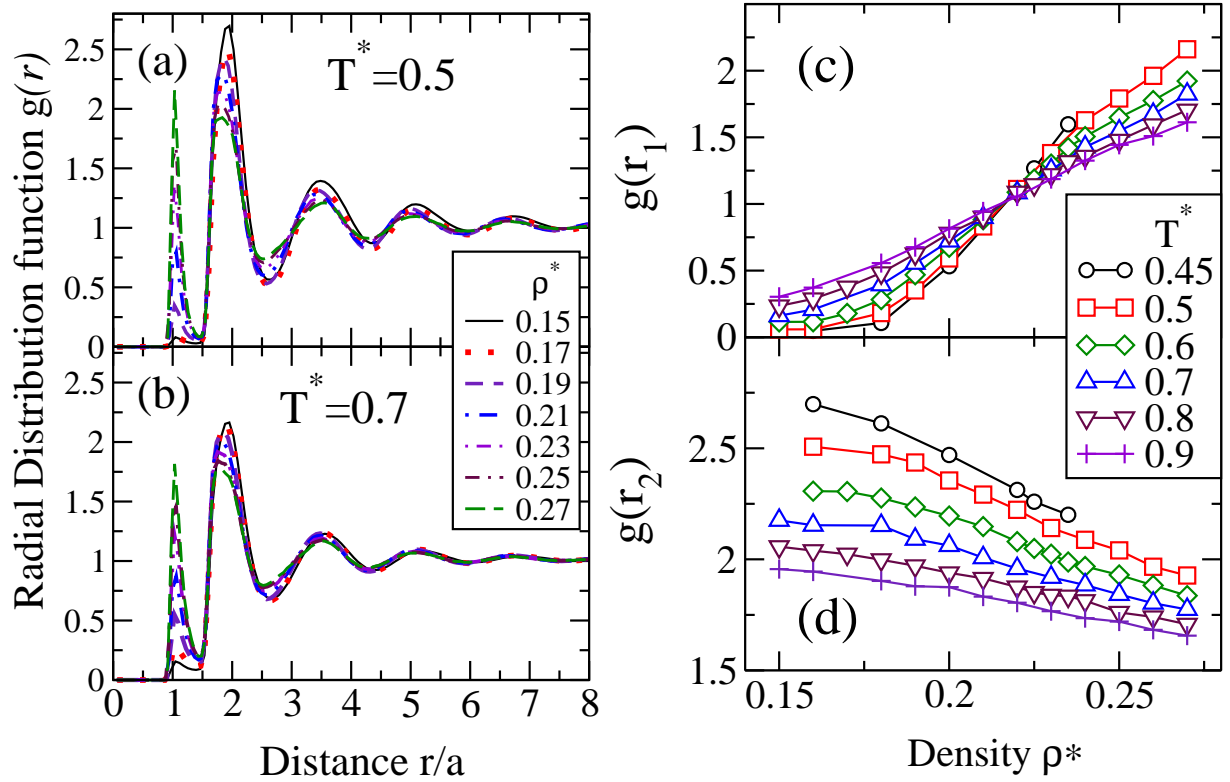


FIG. 10: Change of the radial distribution function $g(r)$ for $\Delta = 30$ with ρ^* and T^* . The $g(r)$ at densities $0.15 \leq \rho^* \leq 0.27$ for (a) $T^* = 0.5$ and (b) $T^* = 0.7$. (c) The height of the first peak of $g(r)$, i. e. $g(r_1)$, always increases for increasing ρ^* , but has a more gradual increase at higher T . (d) The height of the second peak of $g(r)$, i. e. $g(r_2)$, always decreases for increasing ρ^* with a weak dependence on T .

that $\Pi_{1,2}(\rho)$ is not symmetric with respect to the center of the anomalous regions. Instead, $\Pi_{1,2}$ reaches its minimum close to the maximum density with diffusion anomaly (Fig. 12). We also observe that for $\Pi_{1,2}$ there is no clear threshold below which an anomaly appears, contrary to the case of Σ_2 derived from the excess entropy. All these observations suggest that there is no condition on $\Pi_{1,2}$ that is sufficient for the occurrence of the anomalies. More generally, these results suggest also that the onset of the anomalies is related not only to the behavior of the first and second coordination shell of the $g(r)$, but also to the behavior of the higher coordination shells, as recently observed by Krekelberg et al. for other models of anomalous liquids, including water⁶⁰.

To better understand the relevance of the outer shells, following Ref.⁶⁰ we perform an

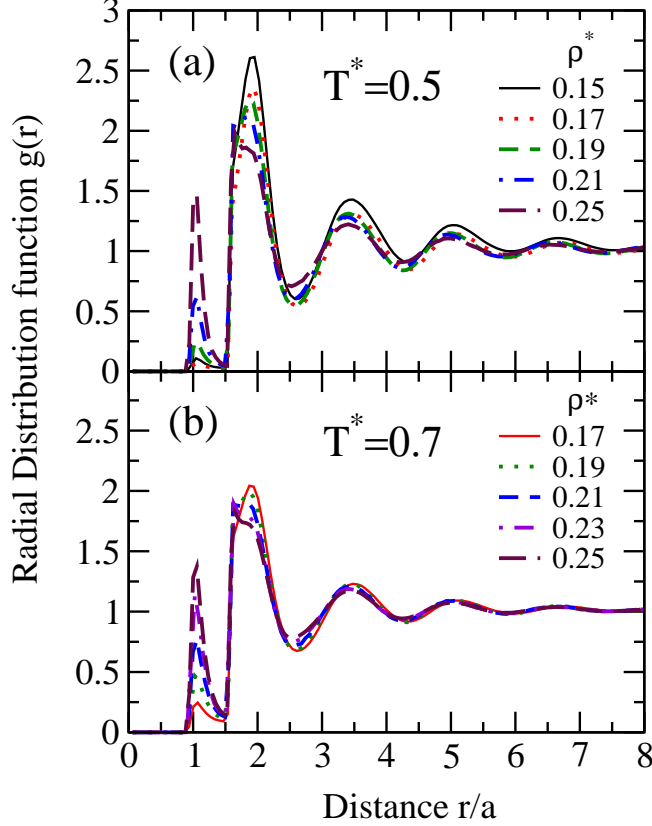


FIG. 11: Radial distribution function $g(r)$ for $\Delta = 500$. For $T^* = 0.5$ (a) and for $T^* = 0.7$ (b) the behaviour of $g(r)$ at different ρ^* is comparable to the case in Fig.10, the main difference being the appearance of a fine structure in the first two peaks at high ρ^* , resembling the $g(r)$ of the DSW potential⁴¹.

analysis of the excess entropy shell by shell, but instead of calculating only the cumulative order integral, as in Ref.⁶⁰,

$$s_2(r) \equiv -2\pi\rho \int_0^r [g(r') \ln g(r') - g(r') + 1] r'^2 dr' \quad (10)$$

here we consider also its derivative

$$\Sigma_2(r) \equiv \left. \frac{\partial s_2(r)}{\partial \ln \rho} \right|_T, \quad (11)$$

where $s_2(r) \rightarrow s_2$ and $\Sigma_2(r) \rightarrow \Sigma_2$ for $r \rightarrow \infty$. Our analysis shows that $\Sigma_2(r)$ presents many oscillations within each coordination shell (Fig. 13, Fig. 14). In several cases different shells contribute with a different sign to the total Σ_2 and in some cases the relevant contribution to the large- r value of $\Sigma_2(r)$ comes from the third or higher coordinations shell.

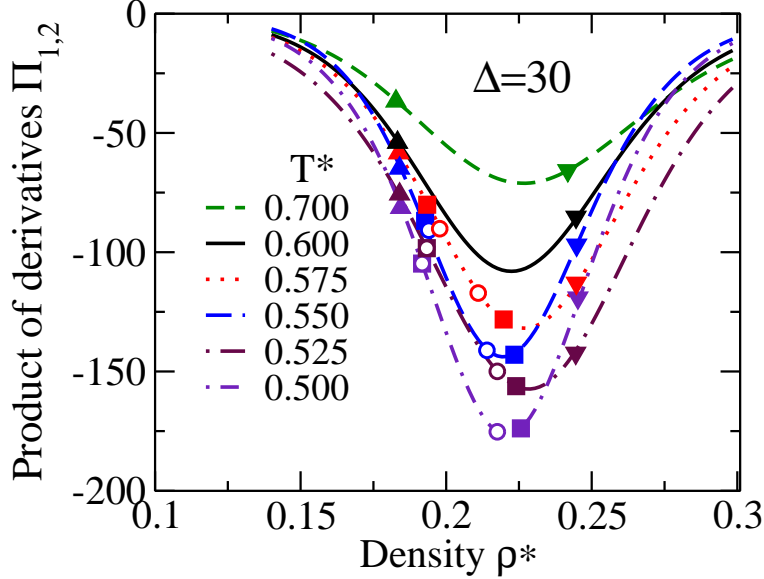


FIG. 12: Product $\Pi_{1,2}$ in Eq.(9) as a function of density for $\Delta = 30$ and different temperatures. Symbols mark the lowest and the highest density where at each T a specific anomaly is observed: \blacktriangle for the maximum Q_6 and \blacktriangledown for the minimum t , marking the structural anomaly region, \blacksquare for the limits of the diffusion anomaly region, \circ for the limits of the density anomaly region. For other values of Δ , not shown here, we find the same qualitative behavior.

For example, in the case with $\Delta = 30$ we observe that at low density (Fig. 13a,c for $T^* = 0.5$ and 0.7 , respectively) the major contribution to the structural anomaly comes from the first and the second shell, although for $\rho^* = 0.17$ at $T^* = 0.7$ (Fig. 13c) it is only after the fourth shell that $\Sigma_2(r)$ stops to oscillate around the threshold for the structural anomaly. On the other hand, the relevance of the third and higher coordination shells is very evident at higher density (Fig. 13b,d), where the sign of $\Sigma_2(r)$ changes in some cases within the third shell ($\rho^* = 0.24$ at $T^* = 0.5$, $\rho^* = 0.23$ and $\rho^* = 0.24$ at $T^* = 0.7$).

Also for the diffusion and the density anomaly, the relevance of the outer shells is evident, especially at high ρ . For example, in Fig. 13b there are several cases where the thresholds for diffusion and density anomaly are reached only within the third shell. While in the majority of cases $\Sigma_2(r)$ saturates within the first fifth shells, we observe also cases where the sixth and possibly higher coordination shells are relevant for the final value of Σ_2 , e. g. for $\rho^* = 0.24$ and $\rho^* = 0.25$ at $T^* = 0.5$ (Fig. 13b) with respect to the empirical thresholds for the density anomaly and the diffusion anomaly, respectively. Therefore, in general is not

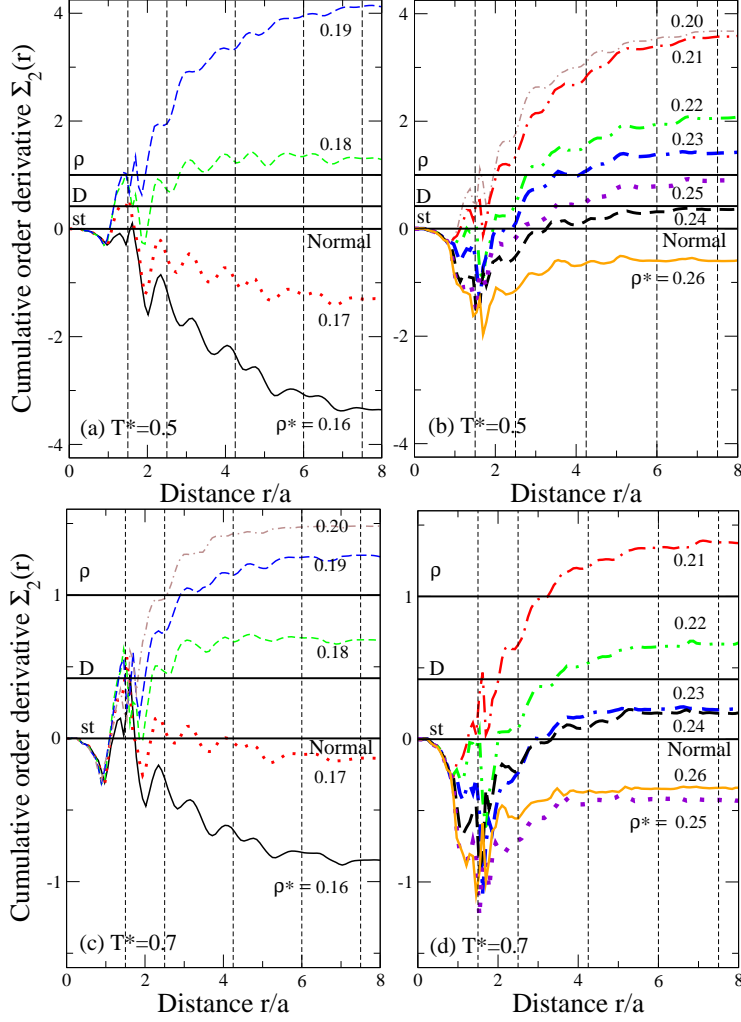


FIG. 13: The cumulative order derivative $\Sigma_2(r)$ calculated for the case $\Delta = 30$, for different temperatures and densities. (a) For $T^* = 0.5$ and density going from $\rho^* = 0.16$ (lower line) to $\rho^* = 0.19$ (upper line). (b) For $T^* = 0.5$ and density going from $\rho^* = 0.20$ (upper line) to $\rho^* = 0.26$ (lower line). (c) For $T^* = 0.7$ and density going from $\rho^* = 0.16$ (lower line) to $\rho^* = 0.20$ (upper line). (d) For $T^* = 0.7$ and density going from $\rho^* = 0.21$ (upper line) to $\rho^* = 0.26$ (second lower line). The values of ρ^* are indicated by the labels near the calculated lines. Horizontal continuous lines with labels *st*, *D* and ρ mark the thresholds for structural anomaly, diffusion anomaly, and density anomaly, respectively. Vertical dashed lines mark the coordination shells as defined by the minima of $g(r)$ in Fig. 10a,b.

possible to establish the occurrence of the anomalies on the base of the local structure (first and second shell), but it is necessary the structural information at much larger scale (forth and outer shells).

From Fig. 13c,d we observe that the empirical thresholds for diffusion anomaly and density anomaly fail to predict correctly the absence of these anomalies at $T^* = 0.7$. The comparison with Fig. 3b, indeed, shows that these anomalies are not found at $T^* = 0.7$, while the calculation of $\Sigma_2(r)$, over more than two coordination shells, would predict the occurrence of the diffusion anomaly for $0.17 < \rho^* < 0.23$ and of the density anomaly for $0.18 < \rho^* < 0.22$ (Fig. 13c,d). Nevertheless, note that the scale in Fig. 13c,d is 40% smaller than in Fig. 13a,b and $\Sigma_2(r)$ never exceeds 1.5.

The same analysis for $\Delta = 500$ presents even more striking oscillations of $\Sigma_2(r)$ within the first two coordination shells (Fig. 14). This is, for example, evident for $\rho^* = 0.19$ and $T^* = 0.7$ (Fig. 14c) at $r/a = 1.5$, where the sudden change of slope of the penetrable soft-core gives rise to a large negative contribution to $\Sigma_2(r)$. However, the contribution of the outer shells leads to positive Σ_2 . At the same T^* and higher ρ^* , similar discontinuities at $r/a = 1.5$ lead to negative Σ_2 , as for $\rho^* = 0.25$ (Fig. 14d). A remarkably large positive contribution to Σ_2 at $r/a = 1.5$ is observed at $T^* = 0.5$ and $\rho^* = 0.23$ (Fig. 14b), in correspondence to the limit of the region of structural anomaly (Fig. 3d). However, also in this case the contribution coming from the outer shells is comparable to that coming from the second shell.

For $\Delta = 500$ the system displays structural anomaly at any T , but diffusion and density anomalies are present only below $T^* = 0.5$ (Fig. 3d). Nevertheless, from Fig. 14 we observe that the empirical thresholds of Σ_2 for diffusion and density anomalies fail at any T , as seen for $\Delta = 30$ (Fig. 13) at higher T only. Also for $\Delta = 500$ the higher the T the lower the saturation value of $\Sigma_2(r)$, as for $\Delta = 30$.

Finally, we observe that in all the cases we have analyzed, when $\Sigma_2(r)$ saturates to a value lower than 2.5, both diffusion and density anomalies are not observed. The only possible exception is observed for $\Delta = 500$ at $T^* = 0.5$ and $\rho^* = 0.20$ (Fig. 14a), where $\Sigma_2 = 4$. However, this state point is at the border of the region where both diffusion and density are anomalous (Fig. 3d).

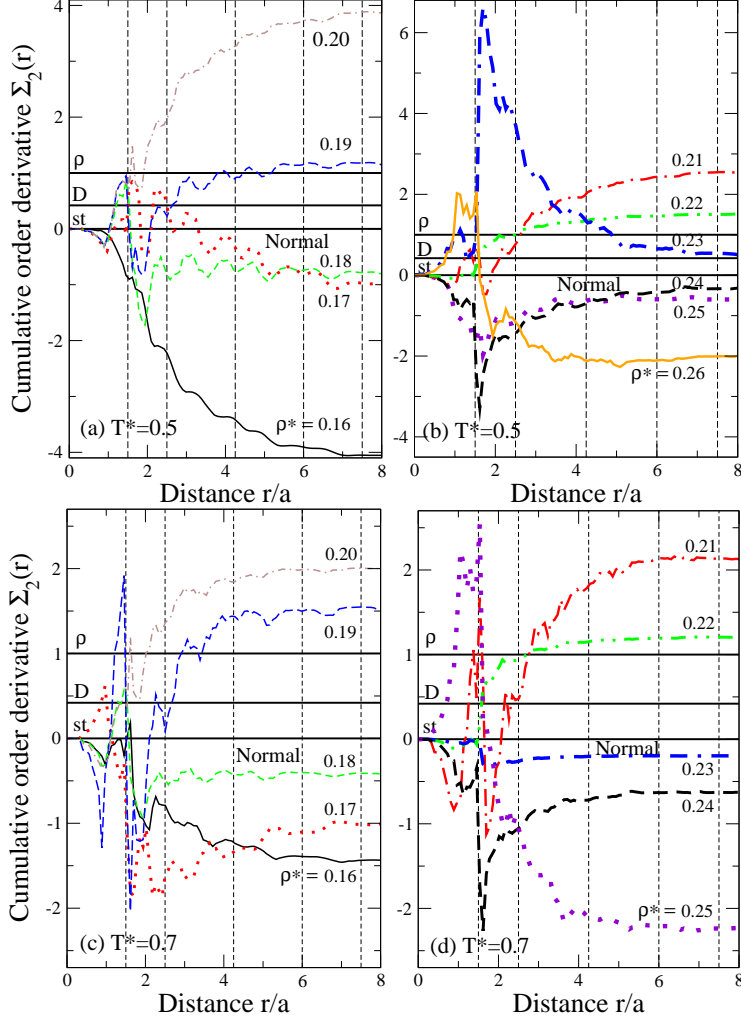


FIG. 14: As in Fig. 13, but for $\Delta = 500$. (a) For $T^* = 0.5$ and density going from $\rho^* = 0.16$ (lower line) to $\rho^* = 0.20$ (upper line). (b) For $T^* = 0.5$ and density going from $\rho^* = 0.21$ (upper line) to $\rho^* = 0.26$ (lower line). (c) For $T^* = 0.7$ and density going from $\rho^* = 0.16$ (lower line) to $\rho^* = 0.20$ (upper line). (d) For $T^* = 0.7$ and density going from $\rho^* = 0.21$ (upper line) to $\rho^* = 0.25$ (lower line). Vertical dashed lines mark the coordination shells as defined by the minima of $g(r)$ in Fig. 11a,b.

VII. SUMMARY AND CONCLUSIONS

We perform a systematic analysis of the soft-core CSW potential⁴⁴ in Eq. (1) by varying the slope Δ of the repulsive shoulder. We consider values from $\Delta = 15$ (smooth and less penetrable at large distance)¹⁴ to $\Delta = 500$ (almost discontinuous and more penetrable at

large distance), we calculate their phase diagrams and the occurrence of the anomalies, and we compare with the results for the discontinuous (DSW) version of the potential⁴⁰.

All the phase diagrams for different values of Δ display at low density the gas-liquid first order phase transition, ending in a critical point C_1 , and at higher density the LDL-HDL first order phase transition, ending in a critical point C_2 . By increasing Δ , both critical points approach the values of the two critical points for the DSW potential (Table I). In this sense, the DSW can be considered as a limiting case of the CSW potential.

For any Δ we observe the occurrence of the density anomaly, diffusion anomaly, and structural anomaly with the same hierarchy as for water^{1,13}, i. e. the density anomaly occurs in the inner region and the structural anomaly in the most external region. The diffusion anomaly region always includes the density anomaly region, being the two regions only slightly separated, with decreasing separation for decreasing ρ and increasing Δ (Fig. 3).

The region of structural anomaly is always present and almost independent of the value of Δ . It slightly contracts toward a limiting finite region for increasing Δ . On the other hand, the regions of diffusion and density anomalies narrow for increasing Δ . A similar behavior has been found recently for purely repulsive soft-core potentials⁶¹. Our finding gives a rationale for the absence of density anomaly for the DSW potential⁴⁰⁻⁴³, here seen as the limit of the CSW for $\Delta \rightarrow \infty$.

We find that the excess entropy analysis gives an approximate estimate of the anomalous regions. However, comparison with Ref.¹⁴ shows that the behaviour of Σ_2 for the DSW potential is still far from what we obtain for $\Delta = 500$, consistent with a slow convergence of the CSW toward the DSW potential when Δ is increased.

We tested some ideas recently suggested as possible explanations for the anomalous behavior of other soft-core potentials. First, we generalized to our CSW potential the Yan et al.⁵⁸ criterion for the occurrence of the diffusion and density anomalies in ramp-like potentials with two characteristic length-scales. To this goal we propose to use as effective length-scales the distances of maxima of the first and second peak of $g(r)$ within the HDL phase. While Yan et al. criterion does not apply to our CSW potentials, our generalized criterion is consistent with our data for different values of Δ and is possibly valid for other continuous potentials with competing length-scales.

Next, we observe that the condition in Eq. (9) proposed by de Oliveira et al.⁵⁹ is not enough to mark the occurrence of the anomalies. This condition relies on the structural

changes of the first and second coordination shell, while from our calculations we conclude that the occurrence of anomalies is related to long range structural changes. To show this result we consider the derivative $\Sigma_2(r)$, Eq. (11), of the cumulative order integral introduced by Krekelberg et al.⁶⁰. The study of $\Sigma_2(r)$ shows that the anomalous behavior of the potential is dominated at high ρ and low T by the structural changes up to the fourth coordination shell, and possibly by even outer shells. We observe that by increasing Δ (more penetrable and sharp soft-core) the contribution to Σ_2 from the first and second shell becomes more relevant. We conclude that the gradual disappearing of the anomalies for large Δ is regulated by the appearance of a more structured short-range order (first and second coordination shell) that dominates over the effect of the larger-range structure.

Acknowledgements

We thank for financial support the Spanish Ministerio de Ciencia e Innovación Grants No. FIS2009-10210 (co-financed FEDER).

* Electronic address: pvilaseca@correu.ffn.ub.es, gfranzese@ub.edu

- ¹ C. A. Angell, E. D. Finch, and P. Bach, *J. Chem. Phys.* **65**, 3065 (1976).
- ² Periodic table of the elements, <http://periodic.lanl.gov/default.htm>, 2007.
- ³ H. Thurn and J. Ruska, *J. Non-Cryst. Solids* **22**, 331 (1976).
- ⁴ G. E. Sauer and L. B. Borst, *Science* **158**, 1567 (1967).
- ⁵ S. J. Kennedy and J. C. Wheeler, *J. Chem. Phys.* **78**, 1523 (1983).
- ⁶ T. Tsuchiya, *J. Phys. Soc. Jpn.* **60**, 227 (1991).
- ⁷ C. A. Angell, R. D. Bressel, M. Hemmatti, E. J. Sare, and J. C. Tucker, *Phys. Chem. Chem. Phys.* **2**, 1559 (2000).
- ⁸ R. Sharma, S. N. Chakraborty, and C. Chakravarty, *J. Chem. Phys.* **125**, 204501 (2006).
- ⁹ M. S. Shell, P. G. Debenedetti, and A. Z. Panagiotopoulos, *Phys. Rev. E* **66**, 011202 (2002).
- ¹⁰ P. H. Poole, M. Hemmati, and C. A. Angell, *Phys. Rev. Lett.* **79**, 2281 (1997).
- ¹¹ S. Sastry and C. A. Angell, *Nature Mater.* **2**, 739 (2003).
- ¹² P. J. Steinhardt, D. R. Nelson, and M. Ronchetti, *Phys. Rev. B* **28**, 784 (1983).

- ¹³ J. R. Errington and P. D. Debenedetti, *Nature (London)* **409**, 318 (2001).
- ¹⁴ A. B. de Oliveira, G. Franzese, P. A. Netz, and M. C. Barbosa, *J. Chem. Phys.* **128**, 064901 (2008).
- ¹⁵ P. C. Hemmer and G. Stell, *Phys. Rev. Lett.* **24**, 1284 (1970).
- ¹⁶ G. Stell and P. C. Hemmer, *J. Chem. Phys.* **56**, 4274 (1972).
- ¹⁷ P. Debenedetti, *Metastable liquids: concepts and principles*, Princeton University Press, Princeton,, New York, 7th edition, 1998.
- ¹⁸ M. Silbert and W. Young, *Phys. Lett.* **58A**, 469 (1976).
- ¹⁹ D. Levesque and J. Weis, *Phys. Lett.* **60A**, 473 (1977).
- ²⁰ J. Kincaid and G. Stell, *Phys. Lett.* **65A**, 131 (1978).
- ²¹ F. Stillinger and T. Weber, *J. Chem. Phys* **68**, 3837 (1978).
- ²² W. Shyu, J. Wehling, M. Cordes, and G. Gaspari, *Phys. Rev. B* **4**, 1802 (1971).
- ²³ P. Debenedetti, V. Raghavan, and S. Borick, *J. Phys. Chem.* **95**, 4540 (1991).
- ²⁴ F. Stillinger and T. Head-Gordon, *Phys. Rev. E* **47**, 2484 (1993).
- ²⁵ S. Borick, P. Debenedetti, and S. Sastry, *J. Phys. Chem.* **99**, 3781 (1995).
- ²⁶ T. Truskett, P. Debenedetti, S. Sastry, and S. Torquato, *J. Chem. Phys.* **111**, 2647 (1999).
- ²⁷ M. Sadr-Lahijany, A. Scala, S. Buldyrev, and H. Stanley, *Phys. Rev. Lett.* **81**, 4895 (1998).
- ²⁸ A. Scala, M. Sadr-Linhijany, N. Giovambattista, S. Buldyrev, and H. Stanley, *J. Stat. Phys.* **100**, 97 (2000).
- ²⁹ A. Scala, M. Sadr-Linhijany, N. Giovambattista, S. Buldyrev, and H. Stanley, *Phys. Rev. E* **63**, 041202 (2001).
- ³⁰ E. Jagla, *Phys. Rev., E* **58**, 1478 (1998).
- ³¹ E. Jagla, *J. Chem. Phys.* **110**, 451 (1999).
- ³² E. Jagla, *J. Chem. Phys.* **111**, 8908 (1999).
- ³³ E. Jagla, *Phys. Rev., E* **63**, 061501 (2001).
- ³⁴ E. Jagla, *Phys. Rev., E* **63**, 061509 (2001).
- ³⁵ N. B. Wilding and J. Magee, *Phys. Rev., E* **66**, 031509 (2002).
- ³⁶ H. Gibson and N. B. Wilding, *Phys. Rev., E* **74**, 061509 (2006).
- ³⁷ P. J. Camp, *Phys. Rev., E* **71**, 031507 (2005).
- ³⁸ J. Caballero and A. Puertas, *Phys. Rev., E* **74**, 051506 (2006).
- ³⁹ N. V. Gribova, Yu. D. Fomin, D. Frenkel, and V. N. Ryzhov, *Phys. Rev. E* **79**, 051202 (2009).

- ⁴⁰ G. Franzese, G. Malescio, A. Skibinsky, S. V. Buldyrev, and H. E. Stanley, *Nature (London)* **409**, 692 (2001).
- ⁴¹ G. Franzese, G. Malescio, A. Skibinsky, S. Bulderev, and H. Stanley, *Phys. Rev., E* **66**, 051206 (2002).
- ⁴² A. Skibinsky, S. Bulderev, G. Franzese, G. Malescio, and H. Stanley, *Phys. Rev., E* **69**, 061206 (2004).
- ⁴³ A. Skibinsky, S. Bulderev, G. Franzese, G. Malescio, and H. Stanley, *Phys. Rev., E* **69**, 061206 (2004).
- ⁴⁴ G. Franzese, *J.Mol.Liq* **136**, 267 (2007).
- ⁴⁵ D. Frenkel and B. Smit, *Understanding Molecular Simulation*, Academic Press, San Diego, 1st edition, 1996.
- ⁴⁶ M. Allen and D. Tidesley, *Computer Simulation of Liquids*, Oxford University Press, New York, 1st edition, 1989.
- ⁴⁷ J. R. Errington, T. M. Truskett and J. Mittal, *J. Chem. Phys.* **125**, 244502 (2006).
- ⁴⁸ Y. Rosenfeld, *J. Phys.: Condens. Matter* **11**, 5415 (1999).
- ⁴⁹ H. J. Raveché, *J. Chem. Phys.* **55**, 2242 (1971).
- ⁵⁰ H. S. Green, *The Molecular Theory of Fluids*, North-Holland, Amsterdam, 1952.
- ⁵¹ A. Baranyai and D. J. Evans, *Phys. Rev. A* **40**, 3817 (1989).
- ⁵² S. N. Chakraborty and C. Chakravarty, *J. Chem. Phys.* **124**, 014507 (2006).
- ⁵³ J. E. Errington, P. G. Debenedetti, and S. Torquato, *J. Chem. Phys.* **118**, 2256 (2003).
- ⁵⁴ A. B. de Oliveira, P. A. Netz, T. Colla, and M. C. Barbosa, *J. Chem. Phys.* **125**, 124503 (2006).
- ⁵⁵ S. Standaert, J. Ryckebusch, and L. De Cruz arXiv:0907.1856
- ⁵⁶ S.A. Egorov *J. Chem. Phys.* **129**, 024514 (2008).
- ⁵⁷ For $\Delta = 500$ we cannot analyze data at density higher than $\rho^* = 0.25$ for the occurrence of spontaneous crystal nucleation. At density $\rho^* = 0.25$ we observe the coexistence of the LDL phase and, in smaller amount, the HDL phase. As a consequence the $g(r)$ averaged over the entire system reflects the presence of the HDL phase.
- ⁵⁸ Z. Yan, S. V. Buldyrev, N. Giovambattista, P. G. Debenedetti, and H. E. Stanley, *Phys. Rev. E* **73**, 051204 (2006).
- ⁵⁹ P. A. de Oliveira, P. A. Netz, and M. C. Barbosa, *Eur. Phys. J. B* **64**, 481 (2008).
- ⁶⁰ W. P. Krekelberg, J. Mittal, V. Ganesan, T. M. Truskett, *Phys. Rev. E* **77**, 041201 (2008).

⁶¹ P. A. de Oliveira, P. A. Netz, and M. C. Barbosa, *Eurphys. Lett.* **85**, 36001 (2009).